

Josephson diode effect in altermagnet-based s-wave superconductor junction

Yi Jiang(蒋易), Han-Lin Liu(刘翰林), and Jun Wang(汪军)

Citation: Chin. Phys. B, 2025, 34 (**10**): 107803. DOI: 10.1088/1674-1056/add7aa
http://cpb.iphy.ac.cn; http://iopscience.iop.org/cpb

What follows is a list of articles you may be interested in

Valley transport in Kekulé structures of graphene

Juan-Juan Wang(王娟娟) and Jun Wang(汪军)
Chin. Phys. B, 2024, 33 (**1**): 017801. DOI: 10.1088/1674-1056/acf9e3

Refractive index of ionic liquids under electric field: Methyl propyl imidazole iodide and several derivatives

Ji Zhou(周吉), Shi-Kui Dong(董士奎), Zhi-Hong He(贺志宏), Yan-Hu Zhang(张彦虎)
Chin. Phys. B, 2020, 29 (**4**): 047801. DOI: 10.1088/1674-1056/ab75cd

Visible-to-near-infrared photodetector based on graphene-$MoTe_2$-graphene heterostructure

Rui-Xue Hu(户瑞雪), Xin-Li Ma(马新莉), Chun-Ha An(安春华), Jing Liu(刘晶)
Chin. Phys. B, 2019, 28 (**11**): 117802. DOI: 10.1088/1674-1056/ab4576

Efficient doping modulation of monolayer WS_2 for optoelectronic applications

Xinli Ma(马新莉), Rongjie Zhang(张荣杰), Chunhua An(安春华), Sen Wu(吴森), Xiaodong Hu(胡晓东), Jing Liu(刘晶)
Chin. Phys. B, 2019, 28 (**3**): 037803. DOI: 10.1088/1674-1056/28/3/037803

Light absorption coefficients of ionic liquids under electric field

Ji Zhou(周吉), Shi-Kui Dong(董士奎), Zhi-Hong He(贺志宏), Ju-Lius Caesar Puoza, Yan-Hu Zhang(张彦虎)
Chin. Phys. B, 2019, 28 (**1**): 017801. DOI: 10.1088/1674-1056/28/1/017801

Josephson diode effect in altermagnet-based s-wave superconductor junction

Yi Jiang(蒋易), Han-Lin Liu(刘翰林)†, and Jun Wang(汪军)

School of Physics, Southeast University, Nanjing 210096, *China*

(Received 18 March 2025; revised manuscript received 9 May 2025; accepted manuscript online 13 May 2025)

We investigate the possible Josephson diode effect (JDE) in a two-dimensional (2D) nonmagnetic planar s-wave superconductor junction, which is constructed on a spin-collinear d-wave altermagnet (AM) material in the presence of Rashba spin–orbit interaction. It is demonstrated that the JDE is critically dependent on the crystalline axis of the AM relative to the current direction. The $d_{x^2-y^2}$ magnetization symmetry can support a JDE whereas the d_{xy} symmetry does not facilitate it. The JDE efficiency can reach up to 40% and can be adjusted by an additional asymmetric gate voltage applied to the non-superconducting region of the junction, including control of its polarity. Our findings provide an electrical means to control the JDE within a non-magnetic AM-based superconducting junction.

Keywords: Josephson diode effect, altermagnet, d-wave magnetization, Rashba spin–orbit interaction

PACS: 78.20.Jq, 71.70.Fk, 72.80.Vp

DOI: 10.1088/1674-1056/add7aa **CSTR:** 32038.14.CPB.add7aa

1. Introduction

Recently, the altermagnet (AM)[1–11] has been proposed to interpret the magnetic structure of numerous spin-collinear materials like RuO_2, KRu_4O_8, and Mn_5Si_3, sparking a surge of research interests within the community. The AM has been dubbed the third magnetic order phase, along with the conventional ferromagnetic and antiferromagnetic phases. AM materials feature d-wave magnetization with zero macroscopic magnetization since spins in these materials are alternatively arranged in both the crystal structure and the reciprocal space.[1] The compensated spin configuration of AMs is similar to that of conventional antiferromagnets. However, due to the broken Kramer's degeneracy, they can exhibit ferromagnetic metal behavior. Because of the zero macroscopic magnetization, AMs have some advantages over ordinary ferromagnets, such as greater insensitivity to magnetic fields, enhanced stability for data retention, and much faster spin dynamics.[12–15]

The interplay between AM and superconductivity has also been intensively investigated. For instance, Smejkal *et al.*[1] and Mazin[16] have respectively analyzed the possible forms of Cooper pairs in materials with the altermagnetic phase as well as the difference from those in ferromagnetic and antiferromagnetic materials. Sun *et al.*[17] have examined the Andreev reflection at the interface of the AM/S (S, superconductor) junction and clarified the AM effect in comparison with that of the conventional ferromagnet.[18] Beenakker *et al.*[19] studied an s-wave S/AM/S Josephson junction (JJ) and found that the system can exhibit a 0–π state transition even though the AM has no macroscopic magnetization. One of the main influences of the AM on Cooper pair transport is that the transport property strongly depends on the AM crystalline orientation relative to the interface of the AM/S junction. Besides, the AM can almost exert the same influence as the ordinary magnetization. This is surely due to the d-wave symmetry of the AM magnetization, which is anisotropic and depends on the direction of the electron's momentum.[20–22] Cheng and Sun[23] have studied a hybrid JJ of s-wave S/AM/p-wave S and demonstrated that the crystalline axis of the AM material plays a vital role in affecting the supercurrent-phase relationship of the JJ.

The nonreciprocal transport in the superconducting system has recently gathered significant attention ever since the superconducting diode effect (SDE)[24–41] was first observed by Ando *et al.*[24] in an [Nb/V/Ta] superlattice structure. The SDE is analogous to the traditional rectification effect in the semiconductors, referred to as the critical supercurrent flowing in the one direction unequal to the oppositely flowing one. It occurs because of the broken time reversal and inversion symmetry in the superconducting system. This is similar to the semiconductor diode effect as the basic building blocks of the modern electronics due to the asymmetric electrostatic barrier. The subsequent experimental works[25–30] have confirmed the SDE in several superconductor bulk materials, which has further aroused the researchers' interest.

The SDE has also been measured in numerous JJ systems,[31–38] such as the Al/InAs two-dimensional (2D) electron gas/Al junction,[35] highly transparent junctions fabricated on InAs quantum wells,[32] and junctions formed on the type-II Dirac semimetal.[33] Currently, it is widely be-

†Corresponding author. E-mail: hanlinl@seu.edu.cn

© 2025 Chinese Physical Society and IOP Publishing Ltd. All rights, including for text and data mining, AI training, and similar technologies, are reserved.

lieved that the finite-momentum Cooper pairs in the bulk S can explain the SDE. These pairs are generated in helical superconductivity within non-centrosymmetric superconductors, which is often the result of the s-wave superconductivity combined with the Rashba spin–orbit interaction (RSOC) and magnetization (or magnetic field) components.[39–45] The finite-momentum Cooper pairs can also account for observed Josephon diode effect (JDE).[46–54] Davydova *et al.*[46] proposed a universal mechanism for JDE in short-limit Josephson junctions, i.e., the Doppler energy shift of the Andreev bound states (ABSs) caused by finite-momentum Cooper pairings leads to the phase-independent asymmetric supercurrent from the continuum states contributing to supercurrent.

Despite the extensive research on the interplay between AM and superconductivity, and the in-depth investigations into the SDE in various superconducting systems, there remains a gap regarding the potential role of AM in the SDE or JDE. Currently, how the unique properties of AM materials, such as their d-wave magnetization and compensated spin configurations, might influence the rectification effect remains untouched. This motivates us to fill this gap by exploring the possible impacts of AM on the JDE.

In this work, we study the possible JDE in a 2D planar JJ where both the d-wave magnetization of AM and RSOC are taken into account in the whole junction but not confined to the non-S middle region in between two S electrodes. Based on a lattice model and numerical calculations, we find that the system can exhibit a considerable JDE efficiency. Nevertheless, this effect is highly dependent on the crystal axis relative to the supercurrent direction. The $d_{x^2-y^2}$ symmetry AM can promote the possible JDE, whereas the d_{xy} symmetry does not support its emergence. Additionally, we also discovered that the ideal JDE efficiency does not occur in the short-junction limit but in the case of the moderate-length JJ. This enables us to introduce a highly asymmetric gate voltage to further regulate the JDE efficiency. Both its magnitude and polarity can be controlled by the gate voltage.

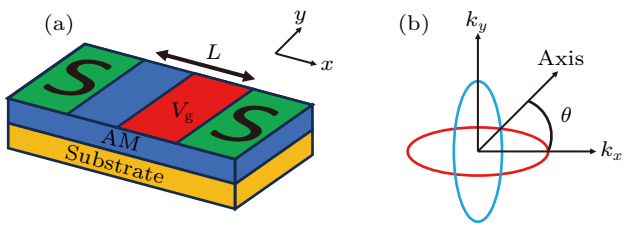


Fig. 1. (a) Setup of a 2D planar Josephson junction. Two S electrodes are put on the AM material and the substrate is supposed to induce RSOC in the AM. A gate voltage V_g is applied to cover a half non-S region to generate an asymmetric electrostatic potential of the JJ. The Junction length is set as L and the current direction is along the x-axis. (b) Two elliptic spin-splitting Fermi surfaces of d-wave magnetization and the $d_{x^2-y^2}$ symmetry are illustrated. The crystalline axis has an angle θ with the momentum k_x.

This work is organized as follows. In Section 2, we present a model to describe the AM-based JJ junction as well as the numerical treatment to the supercurrent. The numerical results are presented in Section 3 and the physics for possible JDE is also discussed. A brief conclusion is drawn in the last section.

2. Model and method

We start from the schematic planar JJ as shown in Fig. 1(a), where the two S electrodes are put onto the 2D surface of an AM while the substrate can induce the RSOC in the AM.[55] It is assumed that the weak superconducting paring potential is induced and distributed uniformly in the left/rigth contacting AM regions through the superconductivity proximity effect. A gate voltage covers the half non-S region ($0 < x < L$) to generate an asymmetric electrostatic potential V_g in the JJ. The current direction is assumed along the x-axis. In the lattice representation, the JJ is described by the following Hamiltonian:

$$\mathcal{H} = H_{2D} + H_{so} + H_{am} + H_S, \tag{1}$$

$$\mathcal{H}_{2D} = \sum_{ij\alpha}[(4t-\mu)C^\dagger_{ij\alpha}C_{ij\alpha} - tC^\dagger_{i+1,j\alpha}C_{ij\alpha} - tC^\dagger_{ij+1,\alpha}C_{ij\alpha} + \text{h.c.}], \tag{2}$$

$$\mathcal{H}_{so} = \sum_{ij\alpha\beta}(\mathrm{i}t_{so}\sigma_y)C^\dagger_{i+1,j\alpha}C_{ij\beta} + (\mathrm{i}t_{so}\sigma_x)C^\dagger_{ij+1,\alpha}C_{ij\beta}, \tag{3}$$

$$\mathcal{H}_{am} = \sum_{ij\alpha\beta}\left(\frac{t_2}{4}\sigma_y C^\dagger_{i+1,j+1,\alpha}C_{ij\beta} - \frac{t_2}{4}\sigma_y C^\dagger_{i-1,j+1,\alpha}C_{ij\beta} + \text{h.c.}\right) + \sum_{ij\alpha\beta}(t_1\sigma_y C^\dagger_{i+1j\alpha}C_{ij\beta} - t_1\sigma_y C^\dagger_{ij+1,\alpha}C_{ij\beta} + \text{h.c.}), \tag{4}$$

$$\mathcal{H}_S = \sum_{ij}\tilde{\Delta}C^\dagger_{ij\alpha}C^\dagger_{ij\bar{\alpha}} + \text{h.c.}, \tag{5}$$

where, $\mathcal{H}_{2D}$ denotes a simple 2D free electron system, $\mathcal{H}_{so}$ is the RSOC term, $\mathcal{H}_S$ represents s-wave Cooper pairing potentials induced in the left and right AM regions just below the two S electrodes through the proximity effect, $\tilde{\Delta} = \Delta\, e^{i\phi_{L(R)}}$, and Δ is the constant pairing strength while $\phi_{L(R)}$ is the superconducting macroscopic phase of the left (right) S region, $\mathcal{H}_{so}$ is the RSOC term which is vital for the possible JDE in the system, otherwise only the 0- or π-state junction can be found but not the ϕ_0-state junction,[18,19] $\mathcal{H}_{am}$ is the d-wave magnetization of the AM.[19] $C^\dagger_{ij\alpha}$ ($C_{ij\beta}$) is the creation (annihilation) operator of electrons in the site ij with spin index $\alpha(\beta)$, $\sigma_{x,y,z}$ is the Pauli matrix, and $\bar{\alpha} = -\alpha$. $i+1$ ($j+1$) represents the nearest neighboring site along x (y) direction of the site i (j). t is the hopping energy between the neighboring sites, t_{so} is the RSOC strength, t_1 and t_2 are hopping term from the AM and given by

$$t_1 = t_{am}\cos 2\theta, \quad t_2 = t_{am}\sin 2\theta, \tag{6}$$

where t_{am} denotes the AM strength, θ is the angle of the crystalline axis related to the current direction as depicted in Fig. 1(b), where the spin-splitting Fermi surface of the AM

material is shown.[1,2] In the low-energy regime, $\mathcal{H}_{\rm am}$ has the following formation:

$$\mathcal{H}_{\rm am} = [t_1 k_x k_y a^2 + t_2(k_x^2 - k_y^2)a^2]\sigma_y, \tag{7}$$

where a is the lattice constant, k_x, (k_y) is the 2D momentum. The first term denotes actually the d_{xy} symmetry of the AM magnetization while the second term represents the $\mathrm{d}_{x^2-y^2}$ symmetry. Generally, the different symmetries give rise to anisotropic transport properties of electrons. Simply, t_1 or t_2 term means different Fermi velocities of electrons for a given momentum (k_x, k_y) as well as corresponding anisotropic Fermi density of states.

We set the magnetization of AM along the y-direction in the spin space because the z-directed magnetization does not lead to the effective nonzero Cooper pairing momentum with the help of the RSOC, while the x-directed magnetization parallel to the current direction does not produce the effective JDE, either[40] It is assumed that the weak superconducting correlation is generated in the left and right S region through superconducting proximity effect, the self-consistent calculation of pair potentials is neglected here and the potential of Δ is set as a constant in numerical calculations for simplicity.

In order to simplify computation of the supercurrent in the planar junction, we can modify the lattice Hamiltonian above into a mixed Bloch-lattice representation, i.e., the y-direction component of Hamiltonian is described in the Bloch representation while the x-component remains in the lattice picture. It reads

$$\begin{aligned}\mathcal{H} = &\sum_{lk_y\alpha\beta}[(4t-\mu-2t\cos k_y a)\sigma_0 + 2t_{\rm so}\sigma_x \sin k_y a - 2t_1\sigma_y\cos k_y a]C^{\dagger}_{lk_y\alpha}C_{lk_y\beta} \\ &+\sum_{lk_y\alpha\beta}\left[-t\sigma_0 + {\rm i}t_{\rm so}\sigma_y - \frac{{\rm i}t_2}{2}\sigma_y \sin k_y a + t_1\sigma_y\right]C^{\dagger}_{l+1,k_y\alpha}C_{l,k_y\beta} + {\rm h.c.} + \sum_{lk_y\alpha}\tilde{\Delta}C^{\dagger}_{lk_y\alpha}C^{\dagger}_{l\bar{k_y}\bar{\alpha}} + {\rm h.c.},\end{aligned} \tag{8}$$

where σ_0 is the unit matrix, l is the x-directed supercell index and k_y is the transverse momentum, $C^{\dagger}_{lk_y\alpha}$ $(C_{lk_y\alpha})$ is the corresponding creation (annihilation) operator of electrons with the site index l, momentum k_y, and spin α. $\bar{k_y} = -k_y$ and $\bar{\alpha} = -\alpha$.

Since the charge current is conserved in the nonsuperconductor region, it can be evaluated in the non-S region of the JJ at any site l as

$$I = \frac{e}{h}\int {\rm d}E \sum_{k_y} {\rm Tr}\{[t_{l,l+1}G^{<}_{l+1,l} - {\rm h.c.}]s_z\}, \tag{9}$$

where $G^{<}_{l,l+1}$ is the lesser Green's function and $G^{<} = (G^{\rm a} - G^{\rm r})f(E)$ in equilibrium, $t_{l,l+1}$ is hopping matrix between two neighboring sites of quasi-one-dimensional lattice model, s_z denotes the z-component of the Pauli operator of the e–h space, the trace is over the spin and Nambu space. $f(E)$ is the Fermi-Dirac distribution function. $G^{\rm r} = (E\sigma_0 - \mathcal{H}_{\rm c} - \Sigma_{\rm L} - \Sigma_{\rm R})^{-1}$ is the retarded Green's function, $G^{\rm a} = [G^{\rm r}]^{\dagger}$, where σ_0 is a unit matrix, $\mathcal{H}_{\rm c}$ is the Hamiltonian describing the middle AM region of the studied JJ in Fig. 1(a), while $\Sigma_{\rm L(R)}$ is the self-energy of the left (right) AM regions contacting with the S electrodes and can be calculated within a usual recursive method.[56]

3. Numerical results of JDE

In numerics, the hopping energy is set as the energy unit $t = 1$ eV, the universal chemical potential is taken as $\mu = 0.2t$, the RSOC strength is set as $t_{\rm so} = 0.1t$, and the ambient temperature is taken as zero, $T = 0$ K. No bias is applied to the system. The superconducting coherence length is estimated to be $\xi = \hbar v_{\rm f}/\Delta \simeq 870a$ with the pair potential set as $\Delta = 0.001t$.

Notice that the RSOC and AM are present in the whole JJ region including both the S electrode and the middle non-S region, unless otherwise stated directly. This consideration stems from the fact that the nonzero Cooper pair momentum in S electrodes induced by AM can result in an effective Doppler energy shift of the Andreev bound states (ABS).[46] This shift accounts for a significant JDE. If the AM is confined in non-S region, the JDE should be rather weak.

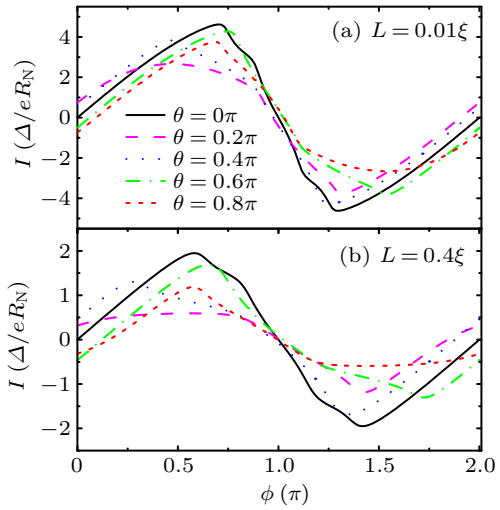


Fig. 2. (a) Supercurrent phase relation $I(\phi)$ with different crystalline axis directions for $L = 0.01\xi$ in panel (a) and $L = 0.4\xi$ in panel (b). Parameters are $t_{\rm am} = 3.5\Delta$ and $t_{\rm so} = 0.1t$, $R_{\rm N}$ is the resistance of the normal junction without superconductivity.

In Fig. 2, the supercurrent-phase relation $I(\phi)$ is plotted within different crystalline axis angles, θ, where $\phi = \phi_{\rm L} - \phi_{\rm R}$ is the superconducting phase difference of the JJ. It is seen that one main characteristic is the ϕ_0 junction emergent in the

system when $\theta \neq 0$, i.e., $I(\phi = 0) \neq 0$. As stated before, the case of $\theta = 0$ corresponds to the pure d_{xy} symmetry AM, this suggests the d_{xy} symmetry does not promote any ϕ_0 junction, let alone the Josephson diode effect (JDE), even though the time reversal and inversion symmetries are broken. Oppositely, once $\theta \neq 0$, the supercurrent at zero phase difference $\phi = 0$ arises and the JDE occurs simultaneously. The case of $\theta = \pi/4$ represents the pure $d_{x^2-y^2}$ symmetry which enables the appearance of the maximum of ϕ_0. It is clearly shown that the positive critical supercurrent I_c^+ is unequal to the opposite one I_c^- when $\theta \neq 0$ from the curves in Fig. 2.

Different JJ's length cases are shown in Figs. 2(a) and 2(b), respectively, while the supercurrent does not show too much deduction with the JJ length, as it is related to the zero macroscopic magnetization of the AM. It is also seen that the supercurrent fulfills the relationship

$$I(\theta + \pi, \phi) = I(\theta, \phi), \tag{10}$$

$$I(\theta) = -I(\pi - \theta, \pi + \phi). \tag{11}$$

The first symmetry directly originates from the AM magnetization in Eq. (6), $t_1 = t_{am}\cos 2\theta$, $t_2 = t_{am}\sin 2\theta$. The second relationship reflects the fact that the critical supercurrent's direction can be reversed by varying the JJ's crystalline axis direction. The JDE efficiency is defined as

$$\eta = \frac{I_c^+ - I_c^-}{I_c^+ + I_c^-}. \tag{12}$$

Here I_c^+ (I_c^-) is the positive or right-flowing (negative or left-flowing) critical supercurrent and can be obtained numerically from the computed $I(\phi)$.

In Fig. 3, the JDE's efficiency versus θ is plotted. One can see that once θ deviates from zero, η rapidly increases. For a short-limit junction (black solid line, $L = 0.01\xi$), the efficiency is almost saturated around $\theta = \pi/4$, while for a moderately long JJ (red dot line, $L = 0.4\xi$), the efficiency has a similar dependence on θ but exhibits a little oscillation due to the resonant effect. Moreover, η satisfies the symmetry

$$\eta(\theta) = -\eta(\pi - \theta). \tag{13}$$

This actually coincides with the supercurrent symmetry relation of Eq. (11). Hence, this formula means $\eta = 0$ when $\theta = 0$, which reflects the d_{xy} AM does not support the JDE even though the necessary components, suitable magnetization, and RSOC, are present in JJ.

For the $d_{x^2-y^2}$ AM in combination with the RSOC, the spin exchange term is given by $[t_m(k_x^2 - k_y^2) + t_{so}k_x]\sigma_y$. This term is asymmetric over the k_x for a fixed transverse momentum k_y. This in turn leads to a nonzero momentum for an s-wave Cooper pair. Actually, the conventional ferromagnetic exchange term can play the same role. Nevertheless, for the d_{xy} AM term, the exchange term becomes $[t_m k_x k_y + t_{so}k_x]\sigma_y$, which is antisymmetric over k_x, this leads to zero mementum Cooper pairs of moving along the x direction, as a result, one can see there is no ϕ_0 junction for the $\theta = 0$ case in Fig. 2 and zero JDE in Fig. 3. It should be noted that the argument is very dependent on the AM magnetization direction, because there is no JDE when the magnetization takes along the x-direction parallel to the current direction.[40] Nevertheless, the d_{xy} symmetry cannot produce the effective nonzero momentum of Cooper pairs in the any case of the AM magnetization.

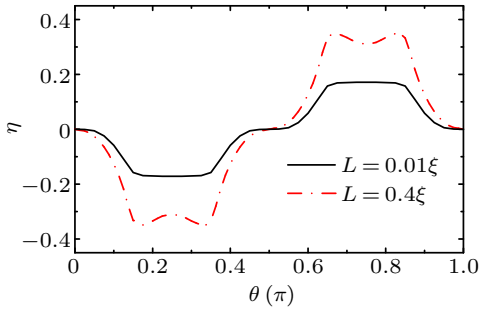


Fig. 3. JDE's efficiency η as a function of the crystalline axis direction θ for different junction lengths. Parameters are the same as those in Fig. 2.

For the JDE mechanism in Fig. 3 still results from the Doppler energy shift of the ABS[46] due to the AM assumed in the S region, and the continuum states produce a phase-independent supercurrent that relies on the nonzero momentum of Cooper pairs. In the following, we plot the ABS to manifest the Doppler energy shift. The ABS can be calculated from the density of states (DOS) of electrons in the junction. The k_y-resolved DOS,[57] $\rho(k_y)$, is given by

$$\rho(k_y, E) = \sum_l \frac{-\mathrm{Im}\, G^r_{ll}(k_y, E)}{\pi}, \tag{14}$$

where $G^r(k_y, E)_{ll}$ is the retarded Green's function of the system, the summation over l is limited in the non-S region ($0 < l < L$) of the JJ where the ABS is supposed to exist.

In Fig. 4(a), we first present the ABS of a short JJ case ($L = 0.01\xi$). The AM is only considered in the non-S region but absent in the S electrodes for comparison. It is seen that the ABS is clearly confined in the energy gap $[-\Delta, +\Delta]$ and there is a zero energy mode at $\phi = \pi$, which reflects the helical superconductivity due to the RSOC. In Fig. 4(b), where the AM is present in the whole JJ instead, the ABS can exhibit an energy shift, i.e., the right- and left-moving states are decoupled to produce two separate bound states and the ABS energies shift away from the superconducting energy gap $[-\Delta, +\Delta]$. According to the Davydova's theory,[46] the ABS energy shift suggests that the continuum states will substantially contribute to the supercurrent, which is independent of the superconducting phase of ϕ but dependent on the current direction (or momentum direction). Therefore, a sizeable JDE arises.

It is generally believed that the maximum of JDE efficiency, η, should appear around $M \sim \Delta$, where M denotes a constant magnetization (in the unit of energy) leading to the nonzero Cooper pair momentum for a single-mode Cooper pair transport,[52] i.e., when the effective energy gap due to the ABS energy's shift almost closes, η may take its maximum but it will decrease monotonically when M overweighs Δ. However, this is not the case for the studied S/AM/S junction here, because the d-wave magnetization is not a constant but dependent on the momentum (k_x, k_y). The different transverse modes (k_y) denote different magnetization strengths so that the average magnetization should be much lesser than the maximum strength of AM, $t_{\rm m}$. Therefore, one can see that in Fig. 4(b), the effective gap does not close even for $t_{\rm am} = 3.5\Delta$, i.e., one set of ABS does not entirely exist in positive or negative energy regimes as shown in the figure.

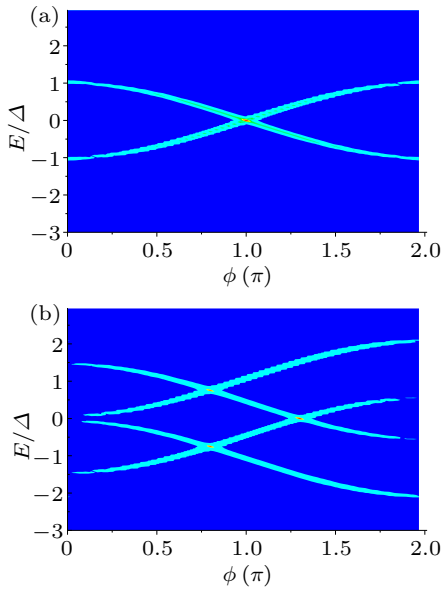


Fig. 4. ABS of the JJ for the S region without AM in panel (a) and with AM in panel (b). The AM is always present in the middle non-S region. The ABS are represented by the density of states around the supposed energy gap $[-\Delta, +\Delta]$. $t_{\rm am} = 3.5\Delta$, $L = 0.01\xi$, and $k_y = 0$.

In Fig. 5, η is calculated as a function of $t_{\rm am}$ for different junction lengths, $L = 0.01\xi$ and 0.4ξ. It is seen that the resonant η can even amount to as high as 50%. In addition, η does not show the declining tendency with increase of the junction length but instead, the oscillation becomes much more apparent for a longer junction $L = 0.4\xi$. This is very different from the single-mode and constant magnetization (M) case,[52] in which η monotonically decreases with the junction length L. Although $t_{\rm am} = 15.8\Delta$, η is quite large (~ 0.53) but at this time, the supercurrent should be suppressed heavily due to the strong AM magnetization. $I(\phi)$ is plotted in Figs. 5(b) and 5(c) for two cases of the AM strengths. The critical supercurrent for $t_{\rm am} = 15.8\Delta$ is much weaker than the case of $t_{\rm am} = 3.5\Delta$. Nevertheless, the oscillating behavior is much clearer for the long JJ than the short one.

The resonant phenomenon depicted in Fig. 5(a) prompts us to consider the possibility of modulating η by designing an asymmetric electrostatic potential to enhance it. This is because the JDE fundamentally depends on the broken inversion symmetry of JJ. We examine the case of a pure electrostatic gate voltage being applied to the middle non-S region of the JJ, as illustrated in Fig. 1(a). Here, the gate voltage does not span the entire region, thereby breaking the left–right inversion symmetry. In Ref. [58], an asymmetric vortex barrier was investigated to boost the JDE in a particular superconductor thin films, and an efficiency of up to 65% was observed.

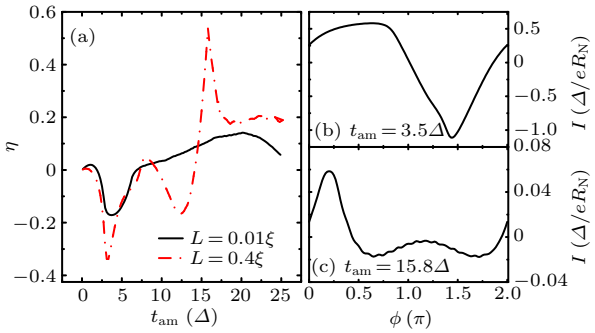


Fig. 5. (a) JDE efficiency as a function of the AM strength $t_{\rm am}$ for different JJ's lengths. Supercurrent phase relation $(I(\phi))$ for two resonant AM strengths for $t_{\rm am} = 3.5\Delta$ in panel (b) and $t_{\rm am} = 15.8\Delta$ in panel (c). Parameters are $L = 0.4\xi$ and $\theta = \pi/4$.

In the calculations, the site energy of the lattice site beneath the gate voltage is assigned a uniform energy shift. In Fig. 6, the relationship between η and $V_{\rm g}$ is presented, and the curve clearly exhibits that η can be significantly modulated by the asymmetric gate voltage $V_{\rm g}$. The noticeable oscillation of η exhibits an approximately symmetric relationship given by $\eta(V_{\rm g}) = \eta(-V_{\rm g})$, which can be attributed to the electron–hole symmetry. More significantly, it can be seen that not only the magnitude of the efficiency but also its polarity can be reversed by $V_{\rm g}$. In other words, the direction of supercurrent diode effect can be controlled by the application of a gate voltage. This can facilitate the JDE's application in the superconductor electronics.

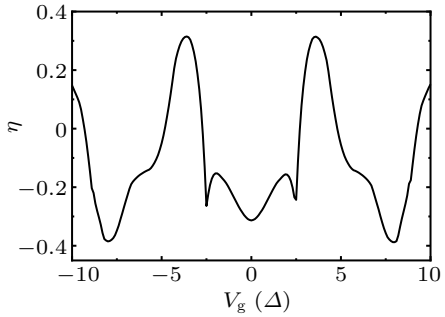


Fig. 6. JDE efficiency versus the asymmetric voltage $V_{\rm g}$. Parameters are $t_{\rm am} = 3.5\Delta$, $L = 0.4\xi$, and $\theta = \pi/4$, while other parameters are described in the text.

4. Conclusion

In summary, we have investigated the Josephson diode effect in a 2D planar superconductor junction based on the

d-wave AM material with the Rashba spin–orbit interaction taken into account. We performed a numerical calculation of the supercurrent as well as the JDE efficiency within a lattice model. It is shown that the direction of the crystalline axis can affect the JDE crucially. The d_{xy}-symmetry AM cannot trigger a diode effect, while the $d_{x^2-y^2}$-symmetry AM can promote it. A sizeable efficiency is not limited to the short-junction limit but exists in a moderately long junction. An external asymmetric gate voltage can be used to control the JDE in terms of both its magnitude and polarity. Our findings provide an electrical means to control the JDE in a nonmagnetic superconducting junction.

Acknowledgements

Project supported by the National Natural Science Foundation of China (Grant No. 12174051) and the Fundamental Research Funds for Central Universities.

References

[1] Šmejkal L, Sinova J and Jungwirth T 2022 *Phys. Rev. X* **12** 031042
[2] Šmejkal L, Sinova J and Jungwirth T 2022 *Phys. Rev. X* **12** 040501
[3] Mazin I and The P R X E 2022 *Phys. Rev. X* **12** 040002
[4] Mazin I 2023 *Phys. Rev. B* **107** L100418
[5] Autieri C 2024 *Nature* **626** 482
[6] Feng Z, Zhou X, Šmejkal L, Wu L, Zhu Z, Guo H, González-Hernández R, Wang X, Yan H, Qin P, Zhang X, Wu H, Chen H, Meng Z, Liu L, Xia Z, Sinova J, Jungwirth T and Liu Z 2022 *Nat. Electronics* **5** 735
[7] Occhialini C A, Martins L G P, Fan S, Bisogni V, Yasunami T, Musashi M, Kawasaki M, Uchida M, Comin R and Pelliciari J 2022 *Phys. Rev. Mater.* **6** 084802
[8] Gonzalez Betancourt R D, Zubáč J, Gonzalez-Hernandez R, Geishendorf K, Šobán Z, Springholz G, Olejník K, Šmejkal L, Sinova J, Jungwirth T, Goennenwein S T B, Thomas A, Reichlová H, Železný J and Kriegner D 2023 *Phys. Rev. Lett.* **130** 036702
[9] Šmejkal L, González-Hernández R, Jungwirth T and Sinova J J 2020 *Sci. Adv.* **6** eaaz8809
[10] Šmejkal L, Hellenes A B, González-Hernández R, Sinova J and Jungwirth T 2022 *Phys. Rev. X* **12** 011028
[11] Shao D F, Zhang S H, Li M, Eom C B and Tsymba E Y 2021 *Nat. Commun.* **12** 7061
[12] Baltz V, Manchon A, Tsoi M, Moriyama T, Ono T and Tserkovnyak Y 2018 *Rev. Mod. Phys.* **90** 015005
[13] Hirohata A, Yamada K, Nakatani Y, Prejbeanu I L, Diény B, Pirro P and Hillebrands B 2020 *J. Magn. Magn. Mater.* **509** 166711
[14] Jungwirth T, Marti X, Wadley P and Wunderlich J 2016 *Nat. Nanotechnol.* **11** 231
[15] Wang H, Lu C, Chen J, Liu Y, Yuan S L, Cheong S W, Dong S and Liu J M 2019 *Nat. Commun.* **10** 2280
[16] Mazin I 2022 arXiv: 2203.05000 [cond-mat.supr-con]
[17] Sun C, Brataas A and Linder J 2023 *Phys. Rev. B* **108** 054511
[18] Papaj M 2023 *Phys. Rev. B* **108** L060508
[19] Beenakker C W J and Vakhtel T 2023 *Phys. Rev. B* **108** 075425
[20] Ouassou J A, Brataas A and Linder J 2023 *Phys. Rev. Lett.* **131** 076003
[21] Zhu D, Zhuang Z Y, Wu Z and Yan Z 2023 *Phys. Rev. B* **108** 184505
[22] Li Y X and Liu C C 2023 *Phys. Rev. B* **108** 205410
[23] Cheng Q and Sun Q F 2024 *Phys. Rev. B* **109** 024517
[24] Ando F, Miyasaka Y, Li T, Ishizuka J, Arakawa T, Shiota Y, Moriyama T, Yanase Y and Ono T 2020 *Nature* **584** 373
[25] Wakatsuki R, Saito Y, Hoshino S, Itahashi Y M, Ideue T, Ezawa M, Iwasa Y and Nagaosa N 2017 *Sci. Adv* **3** e1602390
[26] Hoshino S, Wakatsuki R, Hamamoto K and Nagaosa N 2018 *Phys. Rev. B* **98** 054510
[27] Bauriedl L, Bäuml C, Fuchs L, Baumgartner C, Paulik N, Bauer J M, Lin K-Q, Lupton J M, Taniguchi T, Watanabe K, Strunk C and Paradiso N 2022 *Nat. Commun.* **13** 4266
[28] Itahashi Y M, Ideue T, Saito Y, Shimizu S, Ouchi T, Nojima T and Iwasa Y 2020 *Sci. Adv.* **6** eaay9120
[29] Suri D, Kamra A, Meier T N G, Kronseder M, Belzig W, Back C H and Strunk C 2022 *Appl. Phys. Lett.* **121** 102601
[30] Miyasaka Y, Kawarazaki R, Narita H, Ando F, Ikeda Y, Hisatomi R, Daido A, Shiota Y, Moriyama T, Yanase Y and Ono T 2021 *Appl. Phys. Express* **14** 073003
[31] Wu H, Wang Y, Xu Y, Sivakumar P K, Pasco C, Filippozzi U, Parkin S S P, Zeng Y J, McQueen T and Ali M N 2022 *Nature* **604** 653
[32] Baumgartner C, Fuchs L, Costa A, Reinhardt S, Gronin S, Gardner G C, Lindemann T, Manfra M J, Faria Junior P E, Kochan D, Fabian J, Paradiso N and Strunk C 2022 *Nat. Nanotechnol.* **17** 39
[33] Pal B, Chakraborty A, Sivakumar P K, Davydova M, Gopi A K, Pandeya A K, Krieger J A, Zhang Y, Date M, Ju S, Yuan N, Schröter N B M, Fu L and Parkin S S P 2022 *Nat. Phys.* **18** 1228
[34] Baumgartner C, Fuchs L, Costa A, Picó-Cortés J, Reinhardt S, Gronin S, Gardner G C, Lindemann T, Manfra M J, Faria Junior P E, Kochan D, Fabian J, Paradiso N and Strunk C 2022 *J. Phys.: Condens. Matter* **34** 154005
[35] Gupta M, Graziano G V, Pendharkar M, Dong J T, Dempsey C P, Palmstrm C and Pribiag V S 2023 *Nat. Commun.* **14** 3078
[36] Bocquillon E, Deacon R S, Wiedenmann J, Leubner P, Klapwijk T M, Brüne C, Ishibashi K, Buhmann H and Molenkamp L W 2017 *Nat. Nanotechnol.* **12** 137
[37] Lyu Y Y, Jiang J, Wang Y L, Xiao Z L, Dong S, Chen Q H, Milošević M V, Wang H, Divan R, Pearson J E, Wu P, Peeters F M and Kwok W K 2021 *Nat. Commun.* **12** 2703
[38] Díez-Mérida J, Díez-Carlón A, Yang S Y, Xie Y M, Gao X J, Senior J, Watanabe K, Taniguchi T, Lu X, Higginbotham A P, Law K T and Efetov D K 2023 *Nat. Commun.* **14** 2396
[39] Daido A, Ikeda Y and Yanase Y 2022 *Phys. Rev. Lett.* **128** 037001
[40] Yuan N F Q and Fu L 2022 *Proc. Natl. Acad. Sci. USA* **119** 15 e2119548119
[41] He J J, Tanaka Y and Nagaosa N 2022 *New J. Phys.* **24** 053014
[42] Ilić S and Bergeret F S 2022 *Phys. Rev. Lett.* **128** 177001
[43] Scammell H D, Li J I A and Scheurer M S 2022 *2D Mater.* **9** 025027
[44] Daido A and Yanase Y 2022 *Phys. Rev. B* **106** 205206
[45] Hosur P and Palacios D 2023 *Phys. Rev. B* **108** 094513
[46] Davydova M, Prembabu S and Fu L 2022 *Sci. Adv* **8** eabo0309
[47] Lu B, Ikegaya S, Burset P, Tanaka Y and Nagaosa N 2023 *Phys. Rev. Lett.* **131** 096001
[48] Hu J X, Sun Z T, Xie Y M and Law K T 2023 *Phys. Rev. Lett.* **130** 266003
[49] Steiner J F, Melischek L, Trahms M, Franke K J and Von Oppen F 2023 *Phys. Rev. Lett.* **130** 177002
[50] Souto R S, Leijnse M and Schrade C 2022 *Phys. Rev. Lett.* **129** 267702
[51] Cayao J, Nagaosa N and Tanaka Y 2024 *Phys. Rev. B* **109** L081405
[52] Wang J, Jiang Y, Wang J J and Liu J F 2024 *Phys. Rev. B* **109** 075412
[53] Ding Z, Wang D, Li M, Tao Y and Wang J 2024 *Phys. Rev. B* **110** 155405
[54] Fu P H, Xu Y, Yang S A, Lee C H, Ang Y S and Liu J F 2024 *Phys. Rev. Appl.* **21** 054057
[55] Šmejkal L, MacDonald A H, Sinova J, Nakatsuji S and Jungwirth T 2022 *Nat. Rev. Mater.* **7** 482
[56] Datta S 2000 *Superlattice Microst.* **28** 253
[57] Wang J, Hao L and Liu J F 2016 *Phys. Rev. B* **93** 155405
[58] Hou Y, Nichele F, Chi H, Lodesani A, Wu Y, Ritter M F, Haxell D Z, Davydova M, Ilić S, Glezakou-Elbert O, Varambally A, Bergeret F S, Kamra A, Fu L, Lee P A and Moodera J S 2023 *Phys. Rev. Lett.* **131** 027001